

# Optical smoothing broadens cross beam energy transfer resonance

Y. Lalaire<sup>1-2,\*</sup>, C. Ruyer<sup>1-2,†</sup>, A. Debayle<sup>2-3</sup>, G. Bouchard<sup>1-2</sup>, R. Capdessus<sup>1-2</sup>, A. Fusaro<sup>1-2</sup>, P. Loiseau<sup>1-2</sup>, L. Masse<sup>1-2</sup>, P. E. Masson-Laborde<sup>1-2</sup>, and D. Bénisti<sup>1-2</sup>

<sup>1</sup>CEA, DAM, DIF, F-91297 Arpajon, France

<sup>2</sup>Université Paris-Saclay, CEA, LMCE, 91680 Bruyère-Le-Chatel, France and

<sup>3</sup>Focused Energy GmbH, Im Tiefen See 45, 64293 Darmstadt, Germany

(Dated: March 24, 2026)

We use the theoretical framework introduced in the companion paper to provide simple formulas as regards the resonance conditions for CBET with smoothed laser beams. Our analytical CBET model with optical smoothing shows that these fusion-critical lasers produce a significantly broader resonance than conventional plane wave models predict. In particular, temporal smoothing, as used in many high energy laser facilities, and flow components normal to the CBET ion acoustic waves, significantly modify the power transfer between smoothed beams. Our model predicts that the energy transfer rate out of resonance is substantially higher with optical smoothing than without, a result that has profound implications for optimizing predicting and interpreting future fusion experiments. We provide a simple criterion which pinpoints the laser and plasma parameters for which laser smoothing impacts CBET. These findings pave the way for experimental investigations in high-energy-density physics and fusion energy.

Significant fusion gains demonstrated by the National Ignition Facility (NIF) have driven important research initiatives toward inertial fusion energy (IFE) [1]. The design of these fusion power plants requires highly efficient coupling between the laser drive and the fuel capsule, yet laser-plasma instabilities (LPI) remain a major challenge. LPI scatter pump energy in undesirable directions, reducing the energy coupling efficiency. Among the various LPI, Cross-Beam Energy Transfer (CBET) frequently occurs, impacting capsule symmetry and plasma properties, either in directly [2] or indirectly driven experiments [3, 4]. The prediction and understanding of CBET have been extensively studied, both theoretically [5–9] and experimentally [10–14], with important implications for the design and interpretation of ICF experiments [15–18].

CBET occurs when the crossing of two laser beams with nearly identical wavelengths generates a grating that drives ion acoustic waves (IAWs) in the plasma through the ponderomotive force, driving power exchange between the laser beams. In both directly and indirectly driven capsules, CBET affects the symmetry of implosion and plasma properties [2, 3]. The power transfer is resonant when the phase velocity of the ponderomotive grating matches the sound speed in the plasma rest frame. This condition is met in various scenarios, including when the laser fields are frequency-shifted in a stationary plasma or when the plasma flows at the sound speed in the direction of the laser propagation.

Laser smoothing techniques, such as Random Phase Plates (RPP) and Polarization Smoothing (PS), reduce LPI by degrading the spatio-temporal coherence of the laser. Smoothing by spectral dispersion (SSD) further broadens the temporal spectrum of the laser and dis-

perses spatially the different frequencies across the beam aperture [19–22]. These techniques lead to the formation of micron-scale speckles that evolve over picosecond time scales but are usually ignored for the design (and interpretation) of ICF experiments [3, 16, 23, 24], only accounting for PS. However, the micro-structure of the beams significantly alters the CBET dynamics as shown by recent studies which have improved our understanding of CBET [25–28]. For example, in the case of two RPP beams, the flow-driven grating leads to IAWs confined within the speckle region, while the frequency-shifted case allows the IAWs to propagate beyond the speckle, reducing the maximum power transfer and increasing the resonance width [29].

We use a formalism that, for the first time, fully accounts for both spatial phase plate and temporal spectral dispersion smoothing effects on CBET in realistic geometries. Our model, detailed in the companion paper Ref. [30], reveals previously unsuspected key parameters that dramatically influence power transfer dynamics. Unlike what is usually assumed, we show that drift velocity components normal to the ion acoustic wave direction and the finite coherence time of laser speckles fundamentally alter the wave mixing process, resulting in a resonance broadening beyond plane wave model predictions. This letter uses the theoretical framework detailed in Ref. [30] to identify the critical parameters affecting CBET. We provide simple quantitative criteria based on the resonance width to determine when optical smoothing effects become dominant, with profound implications for interpreting existing experiments and designing future fusion facilities.

The laser modeled here includes smoothing techniques relevant to ICF-relevant facilities. We consider both three dimensional (3D,  $\mathcal{D} = 2$ ) and two dimensional (2D,  $\mathcal{D} = 1$ ) geometries, where the beam first passes through a random phase plate (RPP) composed of  $N^{\mathcal{D}}$  elements, which phase-shift the wavelets randomly. In 3D, these el-

\* [yann.lalaire@cea.fr](mailto:yann.lalaire@cea.fr)

† [charles.ruyer@cea.fr](mailto:charles.ruyer@cea.fr)

elements are indexed in the transverse  $y$  and  $z$  directions, by  $\mathbf{n} = (n_y, n_z)$ , where  $n_y$  and  $n_z$  are integers between 1 and  $N$ . In 2D,  $\mathbf{n} \equiv n_y$ . In addition, the beam is smoothed by SSD. Regarding SSD, the frequency spectrum of the beam is modulated with a frequency  $\omega_d$  and a modulation depth  $M$ . This smoothing introduces an effective bandwidth  $2M\omega_d$  [31]. The beam has a spatial envelope of size  $L$ , a time origin of the SSD frequency modulation  $t_0$  and a polarization vector  $\mathbf{u}$ .

The crossing of two beams induces a ponderomotive grating that drives an acoustic wave on which the light scatters. The  $x$ ,  $y$  and  $z$  axis are set so that the acoustic propagation direction is  $y$  and the  $z$  is normal to the crossing plane. Assuming the paraxial propagation of two laser beams of pulsation and wavevector  $\omega_{1,2}$  and  $\mathbf{k}_{1,2}$ , we first write their ponderomotive beating of pulsation  $\omega = \omega_1 - \omega_2$  and wavevector  $\mathbf{k} = \mathbf{k}_1 - \mathbf{k}_2 \simeq 2k_0 \sin \theta \hat{\mathbf{y}}$  (where  $\theta$  is the crossing angle). We deduce the driven density fluctuations that derives from a linearized (fluid or kinetic) plasma response. We then derive the power exchange, also in the linearized framework, such that the powers of lasers 1 and 2 may be written as  $P_{1/2} = P_{1/2}^0 + \delta P_{1/2}$  where  $\delta P_{1/2} \ll P_{1/2}^0$ . We thus neglect the pump depletion and other non-linear effects such as particle trapping. Following Ref. [29], we then obtain a local value of the intensity exchange which needs to be integrated over the crossing region of extent  $L$  in order to obtain the power exchange,  $\delta P = \delta P_1^0 - \delta P_2^0$ . The two last simplification steps consist in averaging the power exchange on the phase plate variable, owing to the fact that the associated statistical variability is negligible for large enough phase plate element number, as shown in [29] in two dimensions. We also restrict our analysis to temporal average over a modulation period  $2\pi/\omega_d$  of the power exchange and leading to,

$$\begin{aligned} \left\langle \frac{\delta P}{P} \right\rangle_t &= -\frac{CI_2^0}{N^{2D}} \frac{L}{\sin 2\theta} \sum_{\mathbf{n}_1, \mathbf{n}_2} \sum_{m_1, m_2, m_3} J_{m_1} J_{m_2} J_{m_3} \\ &\times J_{m_3+m_2-m_1} e^{-i(m_1-m_3)\omega_d t_0} \\ &\times e^{+i\Psi_{1,m_1,\mathbf{n}_1} - i\Psi_{1,m_3,\mathbf{n}_1} - i\Psi_{2,m_1,\mathbf{n}_2} + i\Psi_{2,m_3,\mathbf{n}_2}} \\ &\times f_K[\omega + (m_1 - m_2)\omega_d, \mathbf{K}_{\mathbf{n}_1\mathbf{n}_2}], \quad (1) \\ C &= (Ze^2\omega_{pe}^2(\mathbf{u}_1 \cdot \mathbf{u}_2)^2)/(2m_i m_e \epsilon_0 k_0 \omega_0^2 c^2 v_g), \\ \mathbf{K}_{\mathbf{n}_1\mathbf{n}_2} &= \{ \sin(\theta)[k_{n_{y1}} + k_{n_{y2}}] \} \hat{\mathbf{x}} + \\ &\{ k - \cos(\theta)[k_{n_{y1}} - k_{n_{y2}}] \} \hat{\mathbf{y}} + \{ k_{n_{z1}} - k_{n_{z2}} \} \hat{\mathbf{z}}, \end{aligned}$$

where  $\epsilon_0$ ,  $v_g$  and  $\omega_{pe}$  are the electric permittivity, the laser group velocity and the electron plasma frequency, respectively. We assumed  $P_1^0 = P_2^0$  for simplicity and introduced  $P = P_1^0 + P_2^0$ , the sound speed  $c_s$  and  $m_{e/i}$  and  $c$ , the electron/ion mass and the light speed in vacuum. The two sums over  $\mathbf{n}$  correspond to the two phase plates of the crossing lasers. The wavevectors  $\mathbf{k}_{\mathbf{n}} = (0, k_{n_y}, k_{n_z})$  are distributed according to the geometry of the beams and depend on the number of elements  $N$ , the f-number  $f_{\#}$ . The two discrete sums over  $m$  stem from the frequency modulation of the two SSD where  $J_m(M)$  is the

Bessel function of the first kind. The phase  $\Psi_{b,m,\mathbf{n}}$  characterizes the spatial dispersion of the different laser frequencies and whose specific form depends on the smoothing technique that is used [30].

The plasma response function is here kinetic,  $f_K(\Omega, \mathbf{K}) = \mathbf{K}^2 \lambda_{De}^2 \chi_e (1 + \sum_i \chi_i) / (1 + \sum_i \chi_i + \chi_e)$  where the subscript  $e$  and  $i$  designate the electrons and the different ion populations which compose the plasma. We also introduced the electrostatic susceptibilities  $\chi_{e/i}$  [32], derived at a wavevector  $\mathbf{K}_{\mathbf{n}_1\mathbf{n}_2}$  and pulsation  $\Omega_{m_1, m_2} = \omega + (m_1 - m_2)\omega_d$ . Note that this power exchange, although averaged on a SSD modulation period, does depend on the time delay between the two SSD frequency modulators,  $t_0$ . Accounting for PS simply consists in replacing  $(\mathbf{u}_1 \cdot \mathbf{u}_2)^2$  by  $1/2$  [33]. The sums in this expression show that the power transfer results from the superposition of the different interactions between the beating electromagnetic wavelets with the driven acoustic wavelets.

This expression is simplified by an average over  $t_0 \in [0, 2\pi/\omega_d]$ , giving,

$$\begin{aligned} \frac{\langle \delta P \rangle_{\phi}^{t, t_0}}{P} &= -\frac{P_2^0 C}{\sin(2\theta) N^{2D}} \sum_{\mathbf{n}_1} \sum_{\mathbf{n}_2} \sum_{m_1} \sum_{m_2} J_{m_1}^2(M) J_{m_2}^2(M) \\ &\times \text{Im} [f_F(\bar{v}_{\phi_{\mathbf{n}_1, \mathbf{n}_2, m_1, m_2}})] . \quad (2) \end{aligned}$$

This step removes the dependence of the power transfer on the spatial frequency dispersion  $\Psi_{b,m,\mathbf{n}}$ . Such simplification leads to relative deviations of the predicted power transfer up to  $\sim 40\%$ , especially in low Landau damped plasmas, as shown in the companion paper Ref. [30]. However, the simplicity of the resulting formula allows to illustrate and analyze the different mechanisms responsible of the deviation of the power transfer from smoothed beams from the plane wave predictions. Similarly, we here use a fluid plasma response,  $f_F(\bar{v}_{\phi}) \approx m_e \omega_{pe}^2 / (m_i c_s^2) / (1 - \bar{v}_{\phi}^2 - 2i \bar{v}_{\phi} \bar{\nu}_L)$ . We introduced the normalized phase velocity of the driven IAWs,  $\bar{v}_{\phi_{\mathbf{n}_1, \mathbf{n}_2, m_1, m_2}} = (\Omega_{m_1, m_2} - \mathbf{K}_{\mathbf{n}_1, \mathbf{n}_2} \cdot \mathbf{v}_d) / (|\mathbf{K}_{\mathbf{n}_1, \mathbf{n}_2}| c_s)$  and  $\bar{\nu}_L = \nu_L / |\mathbf{K}_{\mathbf{n}_1, \mathbf{n}_2}| c_s$ , the normalized Landau damping rate.

The comparison of our model with a kinetic plasma response [Eq. (1)] is made in light of Smilei [34] particle-in-cell (PIC) simulations and is detailed in Ref. [30]. The plasma is composed of  $C^{6+}$  and  $H^+$  ions of equal proportion with a homogeneous density and temperature  $n_e = 0.04n_c$  (where  $n_c \simeq 10^{21} \text{ cm}^{-3}$ ),  $T_e = 2 \text{ keV}$  and  $T_i = 1 \text{ keV}$ . The mean intensity of both P-polarized beams is  $I_0 = 40 \text{ TW/cm}^2$  with a waist of  $L_{\perp} = 48 \mu\text{m}$  and  $t_0 = 0$  for a central laser wavelength of  $1 \mu\text{m}$ . We performed longitudinal SSD corresponding to  $t_0 = 0$ ,  $\omega_d/2\pi = 14.25 \text{ GHz}$  and  $\Psi_{b,m,\mathbf{n}} = f_0(\omega_d/\omega_0) \mathbf{k}_{\mathbf{n}}^2/2k_0$  where  $f_0 = 8 \text{ m}$  is the focal length. Other numerical details can be found in Ref. [30]. Note that we validated the model with paraxial hydrodynamic Hera simulations [35] as detailed in Ref. [30].

When plotted against the resonance parameter  $(\omega - kv_{dy})/(kc_s)$ , the power transfer exhibits a peak of width

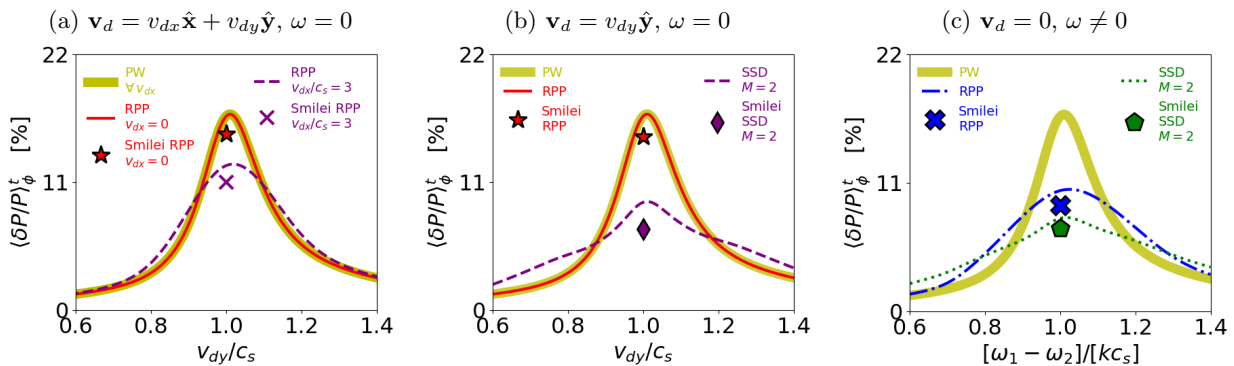


FIG. 1: Power exchange predictions (lines, Eq. (1)) vs plasma conditions: (a,b) drift velocity  $v_{dy}/c_s$  with  $\omega = 0$ , (c) frequency shift  $\omega/kc_s$  with  $\mathbf{v}_d = 0$ . Simulation parameters:  $n_e = 0.04n_c$ ,  $T_e = 2$  keV,  $T_i = 1$  keV,  $f_\# = 8$ ,  $\lambda_0 = 1 \mu\text{m}$ ,  $I_0 = 40$  TW/cm<sup>2</sup> and  $\omega_d/2\pi = 14.25$  GHz. PIC simulation results shown as markers [30].

which depends on the other parameters of the system. We now illustrate the CBET between smoothed beams in three representative situations and examine the dependence of the resonance peak on the flow and optical parameters. The first situation is illustrated in Fig. 1(a) and corresponds to spatially smoothed beams with equal wavelength ( $\omega = 0$ ), without temporal smoothing and crossing in a plasma flowing with velocity  $\mathbf{v}_d = v_{dx}\hat{x} + v_{dy}\hat{y}$ . When  $v_{dx} = 0$ , the RPP curve as a red solid line coincides with the plane wave (PW) limit as a yellow solid line. Indeed, the IAW do not leave the speckle vicinity [29], resulting in a resonance curve of maximum inversely proportional to the damping of the IAW,  $\nu_L$  and of full width at half maximum (FWHM)  $\sigma_L = 2\nu_L/kc_s$  (which is here around  $\nu_L/kc_s \simeq 0.1$ ). The flow component  $v_{dx} = 3c_s$  advects the IAW away from the hot spot regions, thus broadening the resonance and decreasing its maximum, as shown by the purple dashed line. The new resonance width has an additional contribution that can be extracted from our theory. For that, the large phase plate element number limit allows to replace the discrete sums of Eq. (2) by continuous ones. We also write Eq. (2) for a vanishing IAW damping ( $\bar{\nu}_L \rightarrow 0$ ), thus using  $\text{Im}\{f_F(\bar{v}_\phi)\} \approx (\pi/2)\delta(\bar{v}_\phi - 1)$  (where  $\delta(x)$  is the Dirac distribution). Finally, assuming  $f_\# \sin\theta \gg 1$  leads to  $\bar{v}_\phi(\Delta k_X) \approx (v_{dy}/c_s) + \sin(\theta)(v_{dx}/c_s)\Delta k_X/k$  where  $\Delta k_X = k_{ny_1} + k_{ny_2} \in [-2\tilde{k}, 2\tilde{k}]$ . The resulting expression shows explicitly a width of  $\sigma_{v_{dx}} = |v_{dx}|/2f_\#c_s$  (see the supplemental material [36]). For a finite value of the Landau damping, we observe that the total resonance width results from a quadratic sum between the Landau damping and the flow contributions, following  $\sigma^2 \simeq \sigma_L^2 + \sigma_{v_{dx}}^2$ . The markers in Fig. 1(a) correspond to PIC results and confirm our predictions. Likewise, a  $v_{dz}$  flow component further broadens the resonance through the contribution  $\sigma_{v_{dz}} = |v_{dz}|/[2c_s f_\# \sin(\theta)]$ .

The second physical situation corresponds to  $v_{dx} = v_{dz} = 0$  and temporally smoothed laser beams crossing with identical central wavelengths. The effect of temporal smoothing is illustrated by the purple dashed line in

Fig. 1(b) and has, as the previous case, a smaller maximum and a larger width than the plane wave predictions (as a yellow line). Here, the resonance curve has a width related to the laser bandwidth,  $2M\omega_d$  and which is also observed to add quadratically to the plane wave limit according to  $\sigma^2 \simeq \sigma_L^2 + \sigma_{SSD}^2$ . The evaluation of  $\sigma_{SSD}$  requires, as in the previous case, the simplification of Eq. (2) in the low Landau damping and large phase plate element number limits. The laser Bessel temporal spectrum is here replaced by a flat one for simplicity, with a similar procedure as in the previous case [36], we obtain  $\sigma_{SSD} \simeq 2M\omega_d/kc_s$ . Hence, the speckle motion imposed by the SSD effectively smooths the driven density fluctuations, thus decreasing the maximum power transfer, in agreement with the PIC simulations (as markers). Note that our expression of  $\sigma_{SSD}$  remains valid while  $2M\omega_d \lesssim kc_s$  [36].

Figure 1(c) shows the crossing of temporally and spatially smoothed beams with a frequency shift in a plasma at rest ( $\mathbf{v}_d = 0$ ). Without SSD [see the blue curve], the resonance is broadened by the frequency shift. The ponderomotive grating propagates in the laboratory frame, allowing the driven IAW to leave the crossing speckle region. In Ref. [29], assuming a low damping rate, we demonstrate that the resonance width fulfills  $\sigma_{\omega \neq 0} = \delta_{\omega_1, \omega_2}/2|\tan(\theta)|f_\#$  (where  $\delta_{\omega_1, \omega_2}$  is the Kronecker symbol). Hence, the blue line of Fig. 1(c) has a width given by  $\sigma^2 \simeq \sigma_L^2 + \sigma_{\omega \neq 0}^2$ . Adding SSD to the two beams further broadens the resonance as illustrated by the green dotted line and leads to  $\sigma^2 \simeq \sigma_L^2 + \sigma_{\omega \neq 0}^2 + \sigma_{SSD}^2$ . Once again, the power transfer predictions are confirmed by the PIC data as markers.

We demonstrate the spatial smoothing does not impact the CBET resonance when  $\sigma_{\omega \neq 0} \ll \sigma_L$ , specifically, when  $\tan\theta \gg 4f_\#\nu_L/kc_s$ . This is consistent with the CBET measurements performed at large crossing angle that are well reproduced by the plane wave theory [10–12, 37]. Reference [14] presents CBET measurements performed at small angle, but suffers from a target misalignment preventing any quantitative evidence of the impact of

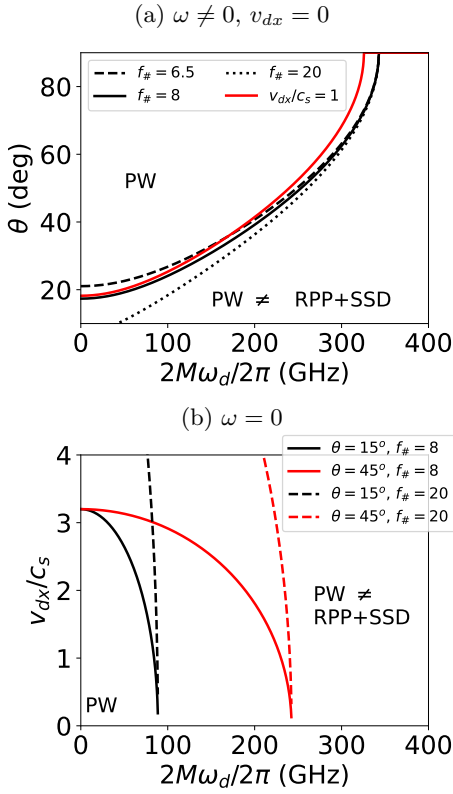


FIG. 2: Threshold [Eq. (3)] for a plasma flow  $\mathbf{v} = v_{dx}\hat{\mathbf{x}} + v_{dy}\hat{\mathbf{y}}$  ( $v_{dz} = \sigma_{v_{dz}} = 0$ ) for a frequency shift (a) and in the drift case (b). The region where plane wave CBET models are (not) satisfactory is noted "PW" ("PW $\neq$ RPP+SSD"). (a) Black lines:  $v_{dx} = 0$  for various f-number; solid red line:  $v_{dx} = c_s$  and  $f_{\#} = 8$ . The lasers have  $\lambda_0 = 0.35 \mu\text{m}$ , we set  $c_s = 10^{-3}c$  and  $\nu_L/kc_s = 0.1$ .

optical smoothing. When accounting for all the physical situations addressed in this letter, SSD,  $v_{dx} \neq 0$  and  $v_{dz} \neq 0$ , we find that laser smoothing modifies the power transfer compared to the plane wave limit when the width of the resonance deviates from the Landau damping. The corresponding threshold which discriminates a case where the power transfer is well reproduced within the plane wave framework from a case which is not is thus,

$$\sigma_{\omega \neq 0}^2 + \sigma_{SSD}^2 + \sigma_{v_{dx}}^2 + \sigma_{v_{dz}}^2 = \sigma_L^2. \quad (3)$$

When the plasma drifts only in the  $y$  direction, this expression gives the crossing angle as a function of the laser bandwidth depending on the laser f-number, as illustrated by the black lines in Fig. 2(a) for  $3\omega$  lasers and a large Landau damping  $\nu_L/kc_s = 0.1$ . This shows that without SSD ( $M\omega_d = 0$ ), CBET at half crossing angle above  $\sim 20^\circ$  is well described by the plane wave limit ("PW"), as shown in Ref. [29]. When adding SSD, the region of parameters where plane wave models are satisfactory shrinks and vanishes for bandwidth above  $\sim 300$  GHz. As a comparison, the NIF frequency

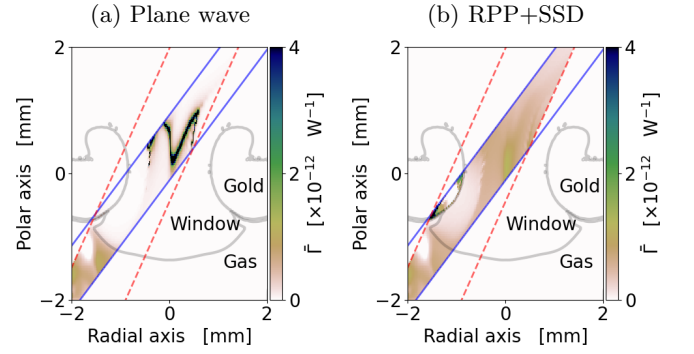


FIG. 3: CBET coupling parameter calculated at the entrance hall of a Troll radiative hydrodynamic simulation of the N210808 NIF shot at 6 ns in the plane wave (a) and smoothed beam (b) cases. The material boundaries are the solid grey lines. The  $30^\circ$  and  $44^\circ$  cone edges are superimposed as dashed red and blue solid lines.

bandwidth at  $3\omega$  used on the N210808 NIF shot [38] is  $\sim 135$  GHz. For LMJ and Omega, the nominal value is 430 and 360 GHz, respectively. As expected, the validity of the plane wave model is larger for large aperture/large speckles ( $f_{\#} = 20$  as a dotted black line) than for small aperture beams ( $f_{\#} = 6.5$  as dashed line). The red solid line considers a plasma drifting with a  $v_{dx}$ -component and with  $f_{\#} = 8$ , it highlights a significant sensitivity of this threshold to the flow direction. The dependence of the CBET model on the  $x$  flow component is illustrated in Fig. 2(b) without frequency shift between the lasers and as a function of the laser bandwidth. Only low  $v_{dx}$  velocities and low bandwidth are well described by a plane wave CBET model. Laser bandwidth above  $\sim 100$  GHz at  $\theta = 15^\circ$  ( $\sim 250$  GHz at  $\theta = 45^\circ$ ) or flows  $v_{dx} \gtrsim 3c_s$  require a CBET model with smoothing ("PW $\neq$ RPP+SSD"). Here again, the range of validity of the plane wave models is larger for large than for small aperture beams.

Regarding the influence of the  $v_{dz}$  component  $\sigma_{v_{dz}} = \sigma_L$  leads to  $|v_{dz}| = 4\nu_L f_{\#} c_s |\sin(\theta)|$ . Consequently, a value of  $v_{dz}$  of the order of the sound speed induces significant discrepancies on the power transfer compared to the PW approximation. This effect may be negligible for large enough laser bandwidth, when  $\sigma_{SSD} > \sigma_{v_{dz}}$ , giving  $2M\omega_d/2\pi \gtrsim k_0 |v_{dz}| / f_{\#} \simeq 240(|v_{dz}|/c_s)$  GHz (for  $c_s = 10^{-3}c$  and  $f_{\#} = 8$ ). To date, this condition for  $v_{dz} = 2c_s$  is not fulfilled in any high energy laser facility. For a facility such as NIF,  $v_{dz} \simeq c_s/2$  is enough to perturb the CBET.

Our theoretical model has been applied to analyze and predict the outcomes of specific experimental setups at the National Ignition Facility (NIF). We performed a detailed Troll radiative hydrodynamic 2D axi-symmetric simulation [39] of the NIF high-yield shot N210808 [40] following Refs. [3, 38]. The CBET coupling parameter

(defined here as  $\bar{\Gamma} = \langle \delta P/P \rangle_t \sin(2\theta)/(LP_2^0)$ ) combined with Eq. (2)) with the specific NIF laser parameters, is illustrated in Fig. 3 at 6 ns during the main laser drive in the crossing region of the 30° and 44° cones. Regarding the laser entrance region, the usual plane wave case presented in panel (a) shows sharp structures located at the CBET resonance. Indeed, the resonance width is dominated here by the local value of the Landau damping frequency. When adding the influence of the optical smoothing, panel (b) presents much broader structures with a resonance width primarily related to the laser bandwidth but also to the laser aperture and flow component normal to the IAWs direction. In this case, the power exchange should be much more gradual than for the crossing of two plane waves, thus modifying the intensity profile of the lasers in the hohlraum.

We have demonstrated the importance of accounting for the influence of temporal smoothing and flow components normal to the IAW direction on the CBET dynamics, under realistic conditions. Our analytical model, based on a linear approach and assuming paraxial approximation detailed in the companion paper Ref. [30], predicts the power transfer depending on the laser smoothing and plasma parameters, which would not be possible with a plane wave model. The use of SSD leads to a broader resonance width and a reduction in the maximum power transfer. Likewise, a misalignment of the

flow with the IAW also results in a broader resonance. We derived simple analytical estimates that allow to pinpoint which laser and plasma parameters require supplementing CBET models with laser smoothing. This suggests that SSD above  $\sim 200$  GHz or  $x$ -flow component above  $\sim c_s$  results in a different power transfer than the usual plane wave predictions depending on the crossing angle and beams aperture. Moreover, the power transfer between smoothed beams is sensitive to a  $z$ -aligned drift velocity component that can arise due to irradiation symmetry defects. In a realistic non-homogeneous plasma, the power transfer resulting from a broader resonance will occur more gradually with optical smoothing than without, significantly changing the intensity profiles and subsequent backscattering and energy deposition properties. Our model also underlines the significant impact of the two SSD modulator synchronization on the CBET outcome, as detailed in Ref. [30]. By accounting for spatial and temporal smoothing, we can more accurately predict and control CBET, paving the way for improved experimental designs and outcomes in ICF research.

This work has been done under the auspices of Commissariat à l’Energie Atomique (CEA), and the simulations were performed using high performance computing resources at Centre de Calcul pour la Recherche et la Technologie and CEA/Tera.

- 
- [1] H. Abu-Shawareb, R. Acree, P. Adams, J. Adams, B. Adis, R. Aden, P. Adrian, B. B. Afeyan, M. Aggleton, L. Aghaian, et al., *Phys. Rev. Lett.* **129**, 075001 (2022).
- [2] R. S. Craxton, K. S. Anderson, T. R. Boehly, V. N. Goncharov, D. R. Harding, J. P. Knauer, R. L. McCrory, P. W. McKenty, D. D. Meyerhofer, J. F. Myatt, et al., *Phys. Plasmas* **22**, 110501 (2015).
- [3] A. Kritcher, C. Young, H. Robey, C. Weber, A. Zylstra, O. Hurricane, D. Callahan, J. Ralph, J. Ross, K. Baker, et al., *Nature Physics* **18** (2022).
- [4] L. Hao, T. Gong, W. Y. Huo, Z. Li, Y. Liu, J. Qiu, Q. Li, H. Zhao, K. Pan, S. Li, et al., *Nat Commun* **16**, 10343 (2025).
- [5] P. Michel, L. Divol, E. Williams, S. Weber, C. Thomas, D. Callahan, S. Haan, J. Salmonson, S. Dixit, D. Hinkel, et al., *Physical review letters* **102**, 025004 (2009).
- [6] D. J. Y. Marion, A. Debayle, P. E. Masson-Laborde, P. Loiseau, and M. Casanova, *Physics of Plasmas* **23**, 052705 (2016).
- [7] A. Debayle, P. E. Masson-Laborde, C. Ruyer, M. Casanova, and P. Loiseau, *Physics of Plasmas* **25**, 052702 (2018).
- [8] S. Huller, G. Raj, W. Rozmus, and D. Pesme, *Physics Of Plasmas* **27** (2020).
- [9] A. G. Seaton, L. Yin, R. K. Follett, B. J. Albright, and A. Le, *Physics of Plasmas* **29**, 042706 (2022).
- [10] C. Neuville, C. Baccou, A. Debayle, P.-E. Masson-Laborde, S. Hüller, M. Casanova, D. Marion, P. Loiseau, K. Glize, C. Labaune, et al., *Phys. Rev. Lett.* **117**, 145001 (2016).
- [11] C. Neuville, K. Glize, P. Loiseau, P.-E. Masson-Laborde, A. Debayle, M. Casanova, C. Baccou, C. Labaune, and S. Depierreux, *Plasma Physics and Controlled Fusion* **60**, 044006 (2018).
- [12] D. Turnbull, A. Colaïtis, A. M. Hansen, A. L. Milder, J. P. Palastro, J. Katz, C. Dorrer, B. E. Kruschwitz, D. J. Strozzi, and D. H. Froula, *Nature Physics* **16**, 181 (2020).
- [13] E. L. Dewald, J. L. Milovich, P. Michel, O. L. Landen, J. L. Kline, S. Glenn, O. Jones, D. H. Kalantar, A. Pak, H. F. Robey, et al., *Phys. Rev. Lett.* **111**, 235001 (2013).
- [14] A. Debayle, P. Loiseau, L. Lecherbourg, P.-E. Masson-Laborde, C. Ruyer, O. Morice, E. Alozy, L. Le-Deroff, T. Caillaud, S. Debesset, et al., *Physics of Plasmas* **32**, 012705 (2025).
- [15] A. Colaïtis, S. Hüller, D. Pesme, G. Duchateau, and V. T. Tikhonchuk, *Physics of Plasmas* **23**, 032118 (2016).
- [16] D. J. Strozzi, D. S. Bailey, P. Michel, L. Divol, S. M. Sepke, G. D. Kerbel, C. A. Thomas, J. E. Ralph, J. D. Moody, and M. B. Schneider, *Phys. Rev. Lett* **118**, 025002 (2017).
- [17] A. Debayle, C. Ruyer, O. Morice, P.-E. Masson-Laborde, P. Loiseau, and D. Benisti, *Physics of Plasmas* **26**, 092705 (2019).
- [18] R. K. Follett, J. G. Shaw, J. F. Myatt, V. N. Goncharov, D. H. Edgell, D. H. Froula, and J. P. Palastro, *Phys. Rev. E* **98**, 043202 (2018).
- [19] T. R. Boehly, V. A. Smalyuk, D. D. Meyerhofer, J. P. Knauer, D. K. Bradley, R. S. Craxton, M. J. Guardalben, S. Skupsky, and T. J. Kessler, *Journal of Applied Physics*

- 85**, 3444 (1999).
- [20] S. Skupsky, R. W. Short, T. Kessler, R. S. Craxton, S. Letzring, and J. M. Soures, *J. Appl. Phys.* **66**, 3456 (1989).
- [21] J. Garnier, L. Videau, C. Gouédard, and A. Migus, *J. Opt. Soc. Am. A* **14**, 1928 (1997).
- [22] J. Garnier and L. Videau, *Phys. Plasmas* **8**, 4914 (2001).
- [23] D. P. Higginson, D. J. Strozzi, D. Bailey, S. A. MacLaren, N. B. Meezan, S. C. Wilks, and G. Zimmerman, *Physics of Plasmas* **29**, 072714 (2022).
- [24] S. Liberatore, P. Gauthier, J. L. Willien, P. E. Masson-Laborde, F. Philippe, O. Poujade, E. Alozy, R. Botrel, G. Boutoux, J. Bray, et al., *Physics of Plasmas* **30**, 122707 (2023).
- [25] A. Oudin, A. Debayle, C. Ruyer, and D. Bénisti, *Phys. Rev. Lett.* **127**, 265001 (2021).
- [26] A. Oudin, A. Debayle, C. Ruyer, and D. Benisti, *Physics of Plasmas* **29**, 112112 (2022).
- [27] A. G. Seaton, L. Yin, R. K. Follett, B. J. Albright, and A. Le, *Physics of Plasmas* **29**, 042706 (2022).
- [28] R. K. Follett, A. Colaïtis, A. G. Seaton, H. Wen, D. Turnbull, D. H. Froula, and J. P. Palastro, *Physics of Plasmas* **30**, 042102 (2023).
- [29] A. Oudin, Y. Lalaire, G. Bouchard, A. Debayle, A. Fusaro, P. Loiseau, C. Ruyer, and D. Benisti, *Physics of Plasmas* **29**, 000000 (2025).
- [30] Y. Lalaire, C. Ruyer, A. Debayle, G. Bouchard, A. Fusaro, P. Loiseau, L. Masse, P. E. Masson-Laborde, and D. Bénisti, in. prep (2025).
- [31] S. Skupsky, R. W. Short, T. Kessler, R. S. Craxton, S. Letzring, and J. M. Soures, *Journal of Applied Physics* **66**, 3456 (1989).
- [32] B. D. Fried, M. Gell-Mann, J. D. Jackson, and H. W. Wyld, *Journal of Nuclear Energy. Part C, Plasma Physics, Accelerators, Thermonuclear Research* **1**, 190 (1960).
- [33] P. Michel, L. Divol, E. A. Williams, C. A. Thomas, D. A. Callahan, S. Weber, S. W. Haan, J. D. Salmonson, N. B. Meezan, O. L. Landen, et al., *Physics of Plasmas* **16**, 042702 (2009).
- [34] J. Derouillat, A. Beck, F. Pérez, T. Vinci, M. Chiaramello, A. Grassi, M. Flé, G. Bouchard, I. Plotnikov, N. Aunai, et al., *Computer Physics Communications* **222**, 351 (2018).
- [35] P. Loiseau, O. Morice, D. Teychenné, M. Casanova, S. Hüller, and D. Pesme, *Phys. Rev. Lett.* **97**, 205001 (2006).
- [36] Y. Lalaire, C. Ruyer, A. Debayle, G. Bouchard, C. R., A. Fusaro, P. Loiseau, P. E. Masson-Laborde, and D. Bénisti, Supplemental material for "cross beam energy transfer with optical smoothing", 2025, Supplemental Material.
- [37] A. M. Hansen, K. L. Nguyen, D. Turnbull, B. J. Albright, R. K. Follett, R. Huff, J. Katz, D. Mastro Simone, A. L. Milder, L. Yin, et al., *Phys. Rev. Lett.* **126**, 075002 (2021).
- [38] A. L. Kritcher, A. B. Zylstra, D. A. Callahan, O. A. Hurricane, C. R. Weber, D. S. Clark, C. V. Young, J. E. Ralph, D. T. Casey, A. Pak, et al., *Phys. Rev. E* **106**, 025201 (2022).
- [39] E. Lefebvre, S. Bernard, C. Esnault, P. Gauthier, A. Grisolle, P. Hoch, L. Jacquet, G. Kluth, S. Laffite, S. Liberatore, et al., *Nucl. Fusion* **59**, 032010 (2018).
- [40] H. Abu-Shawareb, R. Acree, P. Adams, J. Adams, B. Addis, R. Aden, P. Adrian, B. B. Afeyan, M. Aggleton, L. Aghaian, et al., *Phys. Rev. Lett.* **129**, 075001 (2022).